

DARK SPOT DETECTION FOR CHARACTERIZATION OF OIL SPILLS USING POLSAR REMOTE SENSING

Anurag Kulshrestha^{1,2}, Shashi Kumar¹ and Wietske Bijker²

¹Indian Institute of Remote Sensing (IIRS),
Kalidas Road, 248001, Dehradun, India

²Faculty of Geoinformation Science and Earth Observation (ITC), University of Twente,
Hengelostraat 99, 7514 AE, Enschede, The Netherlands

Email: kulshrestha@student.utwente.nl, shashi@iirs.gov.in, w.bijker@utwente.nl

KEYWORDS: SAR Polarimetry, UAVSAR, Markov Random Field

ABSTRACT:

Remote sensing using Synthetic Aperture Radar (SAR) is one of the most commonly used methods for detecting and characterizing oil spills in seas and oceans. However, distinguishing true oil spills from false look-alike features like biogenic oil is a major challenge. The aim of this study is to use polarimetric decompositions like H/A/alpha decomposition to separate oil spill areas from look-alike features using Maximum Likelihood Classification (MLC) and Markov Random Field (MRF) classification methods. The classification algorithm is applied to a quad-polarized Ground Range Detected (GRD) dataset of Uninhabited Ariel Vehicle Synthetic Aperture Radar (UAVSAR) sensor of an experimental oil spill in Norway. The dataset contains a strip of plant oil and three strips of different types of crude oil-water emulsions with varying concentrations of oil. Polarimetric features are extracted using covariance matrix, coherency matrix and H/A/alpha polarimetric decomposition. An MRF classifier is trained and its parameters are optimized over the image. The kappa value in the case of MLC was 0.295 and 0.266 in case of MRF. Using the MRF classifier on features results does not significantly improve classification of different type of oil spills. The confusion between classes increases as the level of dilution in the oil-water emulsion increases. The procedure works well in separating oil spills from water. It also helps to better characterize oil spills which have higher concentration of oil. The incidence angle effect also contributes to the misclassification of oil spills in the area. This can be rectified by applying incidence angle correction.

INTRODUCTION

Oil spill is a release of mineral oil in a water body from offshore drilling rigs, oil tankers or underwater oil pipelines. After getting introduced into the water, oil usually forms a thin film over the water surface which is referred to as oil spill, marine surface slick or oil slick. However, oil spill can also be present as thick layers on the water surface as oil-water emulsions which seldom sink down to the sea bed (Dell'Amore, 2015). The oil spills move both horizontally over the water surface and vertically inside the water. Wind and surface water current are the two major factors responsible for the spread of oil over the water surface. There are several factors which influence the oil spill impact on the environment. Amongst all of them, the crucial ones are its rate and direction of movement, its location relative to human and marine species habitats, its type and its extent over the ocean surface.

Oil spills cause many harmful consequences for the marine and coastal ecosystems (Chang, Stone, Demes, & Piscitelli, 2014). A well-known oil spill event in recent history was the Deepwater Horizon oil spill in 2010. It resulted in 4.9 million barrels of oil getting spilt in the Gulf of Mexico over a period of 5 months (Weber, 2010). It caused a huge impact on the living flora and fauna of the gulf (Beyer, Trannum, Bakke, Hodson, & Collier, 2016). Many animals, including birds, sea turtles, mammals and fishes died as a result of this oil spill (CNN, 2010). It also impacted on the lives of people living along the coast by hampering tourism and fisheries industries of the region. Therefore, it is necessary to anticipate and prepare for oil spills to limit their adverse consequences on the environment.

To curtail the impact of oil spill, it is important to identify its location and characterize it (i.e. to distinguish it from similar look-alike features, e.g. marine algae) as accurately as possible. Early and accurate detection ensures quick and targeted response to the affected location. It also helps in efficient allocation of relief efforts and resources. Moreover, having knowledge about the type of oil getting spilled assists decision makers in choosing the appropriate method for oil spill cleanup. Therefore, there is a demand of efficient and reliable methods for accurate detection and characterization of oil spills.

Active Remote Sensing sensors such as Synthetic Aperture Radar (SAR) is one of the most efficient and widely

used methods in oil spill detection. As compared to passive remote sensing methods such as in visible range (Wang, Pan, Zhan, & Zhu, 2010), infrared (IR) range (Pinel & Bourlier, 2009), near infrared (NIR) range (Bulgarelli & Djavidnia, 2012), and ultraviolet (UV) range, SAR sensors are independent of the sun to collect imagery, and hence also work during night. Moreover, SAR can provide images in all-weather conditions because of the capability of radar waves penetrating through clouds. Therefore, SAR remote sensing is one of the most commonly used methods for detecting and characterizing oil spills (Fingas & Brown, 2014).

SAR remote sensing of sea surfaces is based on the interaction of electromagnetic radar waves with sea surface matter waves. Ocean or sea surfaces are characterized by two types of waves: capillary waves and gravity waves. Capillary waves, also termed as ripples, are short wavelength waves which are formed due to the interaction of water surface with the wind. These waves are sensitive to the surface tension of the fluid surface. Gravity waves are longer in wavelength and are mostly influenced by the effects of fluid inertia and gravity. A slick cover causes dampening of small capillary waves due a reduction in surface tension and decrease in wind friction. This causes a suppression in wave growth and an increase in wave dissipation (Minchew, Jones, & Holt, 2012). Therefore, oil slicks mostly appear darker than the wind-roughened surrounding ocean in the acquired SAR imagery.

In spite of all the advantages which SAR remote sensing offers in detecting oil spills, there are various limitations associated with this technique. These limitations include false target detections such as low wind areas, marine biogenic slicks, rainfall footprints (Alpers, Zhang, Mouche, Zeng, & Wai, 2016), and ship wakes. Marine biogenic slicks behave in a very similar way as mineral oil spills. They also cause dampening of capillary waves resulting in reduction of radar backscatter. These natural slicks are mostly caused due to the presence of algae, biogenic oils, glacial flour, and whale and fish sperm (Gens, 2008). Therefore, detection of mineral oil spills using radar is difficult in areas where the probability of occurrence of above mentioned false targets is high (Liu, Zhao, Li, He, & Pichel, 2010). Polarimetric SAR (Pol-SAR) data has been reported to aid in accurate oil slick detection and in distinguishing between biogenic and anthropogenic mineral oil spills (Gade, Alpers, Hühnerfuss, Masuko, & Kobayashi, 1998).

An increase in the number of polarization channels of SAR datasets (e.g. from dual-pol to quad-pol) increases the number of polarimetric features which can be extracted from the datasets. Use of polarimetric data in ocean monitoring is based on Bragg Scattering Theory (Valenzuela, 1978). The backscatter response from the sea surface waves depends upon the local incidence angle, wavelength of radar waves, wavelength of surface waves, the dielectric constant of the surface material and nature of polarization of incident electromagnetic radar wave. Polarimetric data is used to extract certain polarimetric features which are related to the factors in Bragg scattering theory. Some of the polarimetric features which have been reported to be useful in oil spill detection and in capturing the factors in the Bragg Scattering Theory are complex co & cross-polarization cross product, determinant of sample covariance matrix, entropy (H), anisotropy (A) and angle (α) between the eigenvectors of coherency matrix. The real and imaginary parts of co-polarization cross product are able to capture large scale roughness of the sea surface (Espeseth et al., 2017). Polarimetric target decompositions such as H/A/ α decomposition make use of quad-pol data and are useful in detecting oil spills (Skrunes, Brekke, Jones, & Holt, 2016).

There are many classification methods which can be used to classify oil spills. They include maximum likelihood classifier(MLC), support vector machine(SVM), and Markov Random Fields(MRF) (Lopez & Moctezuma, 2005; Moctezuma, Parmiggiani, & Lopez, 2014; Morales, Moctezuma, & Parmiggiani, 2008). Moreover, PolSAR classification methods, such as Wishart classification have also been used in detecting oil spills (Kumar, Kattamuri, & Agarwal, 2016). MRF based soft classification methods can also be used to classify oil-slicks. The probability of true oil spill detection from SAR data is affected by multiple factors, such as wind speed range, presence of algae in the region, proximity to shipping routes and oil rigs and shape of the slick. These effects are usually represented in a set of different hard classified maps. As an alternative, the factors stated above can be captured by modeling of oil spills as probability surfaces over the 2 dimensional sea surface.

This research aims to use contextual features and polarimetric features derived from quad-polarized Uninhabited Aerial Vehicle Synthetic Aperture Radar (UAVSAR) data to detect and characterize oil spills. For this purpose, this research uses classification methods such as MLC and MRF based classification and compare their performance of the basis their accuracy in classifying oil spills.

STUDY AREA AND DATASET

For this research UAVSAR L-band quad-polarized image acquired over the region of North Sea, Norway on June 10th, 2015 was used. This image acquisition was part of a joint exercise called NORSE-2015, where four different types of oil slicks were intentionally spilled into the sea and data was captured using multiple satellites and the

UAVSAR air-borne sensor (Table-2). These four oil slicks can be observed in Figure-1, and the characteristics of the oil dispersed over the sea is mentioned in Table-1. A series of 22 datasets were collected by the airbourne sensor which spanned over a time period of approximately 8 hours. One of them is the UAVSAR dataset with identification code 'norway_00709_15092_000_150610_L090_CX_01' which was used to carry out this study. A small subset of the image was cropped using PolSARpro software such that the image focused on all the 4 oil spill regions (Figure 1). The cropped image had a longitude and latitude pixel spacing of 0.000111 and -.000055 decimal degrees respectively. The extent of the image was 1431 x 1178 pixels.

This dataset was chosen because of certain advantages associated with the data. This dataset is freely available through NASA-JPL UAVSAR data portal (NASA-JPL, n.d.). It is quad-polarized, has low system noise floor, higher contrast and higher spatial resolution as compared to other data sources which collected images of the same oil spill (Skrunes et al., 2016). Moreover, the SAR image contains four different types of oil spills which could be used to develop a versatile oil spill detection model.

Table 1: Details of emulsions spilt in NORSE-2015 exercise (Brekke et al., 2016)

<u>Release</u>	<u>Quantity (litres)</u>	<u>Specification</u>
Emulsion 3	500	80% oil and 20% sea-water
Emulsion 2	500	60% oil and 40% sea-water
Emulsion 1	500	40% oil and 60% sea-water
Plant Oil	200	100% plant oil

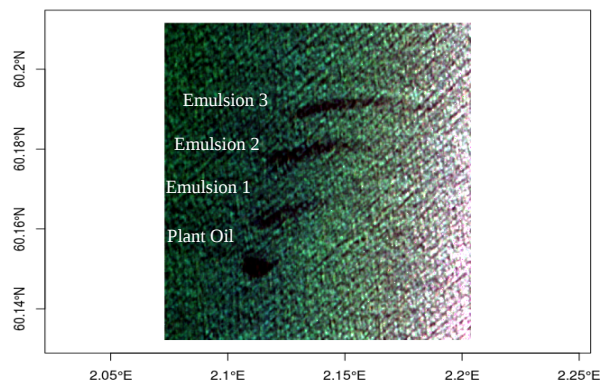


Figure 1: Pauli RGB image of subset of UAVSAR PolSAR image of NORSE-2015 oil spill. R → C11, G → C22, B → C33

Table 2: Details of UAVSAR sensor which acquired images of oil spills in NORSE-2015 exercise (Skrunes et al., 2016).

Sensor	UAVSAR
Frequency	L band (1.2175 - 1.2975 GHz)
Type	GRD
Polarization	Quad-Pol
Incidence angle range	25 – 65 degrees
Longitudinal Spatial Resolution	11.111e-05 degrees
Latitudinal Spatial Resolution	5.556e-05 degrees
Date and Time acquisition	10-June-2015, 11:45:40 UTC
Radiometrically corrected?	Yes

METHODOLOGY

Preprocessing

As a preprocessing step, speckle filtering was performed on the dataset using Lee sigma filter (Espeseth et al., 2017). The sigma value was chosen to be 0.9, target and filter window size were 3 and 9 respectively. Thereafter, the covariance matrix elements were extracted using PolSARpro software.

Feature Extraction

The polarimetric features used for the classification were real and imaginary parts of co-polarization cross product, co-polarization intensities ($S_{VV}S_{VV}^*$ and $S_{HH}S_{HH}^*$), cross polarization intensity ($S_{HV}S_{HV}^*$), real and imaginary parts of two co-cross polarization cross product ($S_{HH}S_{HV}^*$ and $S_{HV}S_{VV}^*$). Five classes were identified and used for further analysis. These classes were Sea, Plant Oil, Emulsion-1, Emulsion-2 and Emulsion-3. The training and testing areas for the classification were delineated using QGIS software. These training and testing areas can be observed in Figure 2 and the number of pixels from image in respective areas can be noted from Table 3.

MLC and MRF based classification

R programming language was used to read the features, training areas, and testing areas. Furthermore, the classifications were also performed in R. The data in the features did not exactly follow Gaussian distribution but was assumed to be distributed normally. This can be observed in Figure 3 which depicts the data distribution of co-polarization (VV) intensity. Class separability measures were calculated using transformed divergence method. Thereafter, MLC was performed on the dataset with the assumption that the conditional probability term in MLC and maximum a-priori (MAP) solution followed normal distribution.

Subsequently, MLC based MRF classification was performed on the set of features described in the previous paragraph. The parameters of the MLC based MRF classifier were optimized on a small subset of the image.

Post classification accuracy assessment was performed and hence, the performance of both MLC and MLC based MRF classifier were compared using their corresponding confusion matrices.

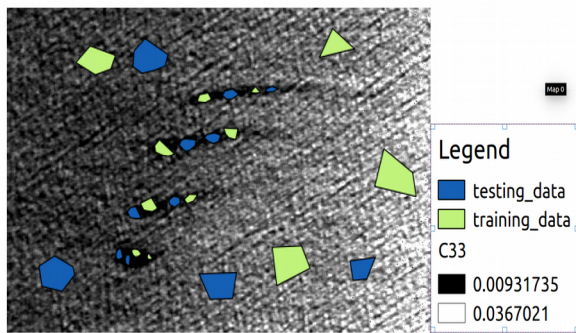


Figure 2: Training and testing areas for the classifier

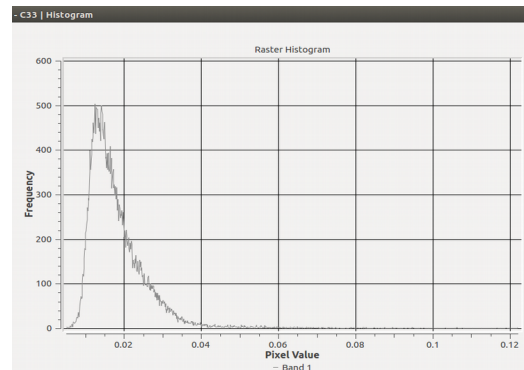


Figure 3: Data distribution of VV intensity feature

Table 3: Number of pixels from image in training and testing areas

	Emulsion-1	Emulsion-2	Emulsion-3	Plant Oil	Sea
Number of pixels in training set	2707	3583	1574	902	40586
Number of pixels in test set	1337	4307	1853	1167	35017

RESULTS AND DISCUSSION

Class separability measures which were calculated using transformed divergence method are reported in Table 4. It can be observed from the measures that as the concentration of oil in the emulsions increase, the class separability values between oil slicks also increase. This result correlates well with the information about the concentration of different oil slicks. Less concentration of oil in the slicks results in an increase in its similarity with water. It is also interesting to note that it is difficult to distinguish emulsion 1 - emulsion 2 and emulsion 2 - emulsion 3 combinations.

The classification result after performing MLC on the dataset is displayed in Figure 4. The overall accuracy and kappa values came out to be 82.43% and 0.295 respectively. The confusion matrix obtained from maximum likelihood classification results and the test data are reported in Table 5. It can be observed from these results that error of omission in classification are lower for classes Sea, Plant Oil and Emul-3 classes as compared to the other

classes. The class Sea is most efficiently classified by this classification method. The high number of misclassifications for classes Emul-1 and Emul-2 resulted in a low kappa value .

Table 4: Class Separability (Transformed Divergence)

	Emul-1	Emul-2	Emul-3	Plant Oil	Sea
Emul-1	0	0.59	1.35	1.86	2
Emul-2	0.59	0	1.09	1.94	2
Emul-3	1.35	1.09	0	1.96	2
Plant Oil	1.86	1.94	1.96	0	2
Sea	2	2	2	2	0

Table 5: Confusion Matrix (MLC)

	Emul-1	Emul-2	Emul-3	Plant Oil	Sea
Emul-1	40	549	86	164	4
Emul-2	19	851	505	549	68
Emul-3	0	40	89	0	2
Plant Oil	0	6	0	84	0
Sea	1278	2861	1173	370	34943

Table 6: Confusion Matrix (MLC-MRF)

	Emul-1	Emul-2	Emul-3	Plant Oil	Sea
Emul-1	39	538	80	226	14
Emul-2	23	752	435	541	58
Emul-3	0	2	59	0	0
Plant Oil	0	1	0	35	0
Sea	1275	3014	1279	365	34945

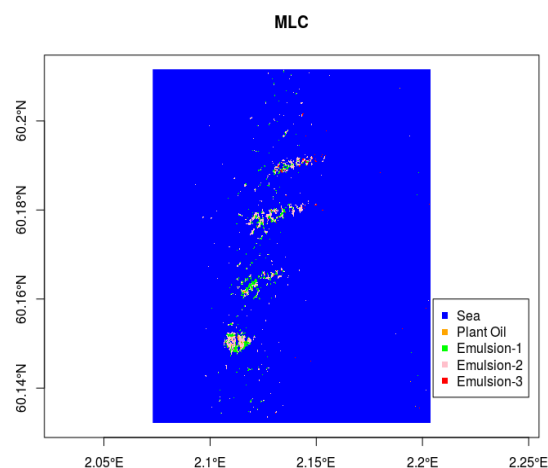


Figure 4: Classification results from MLC

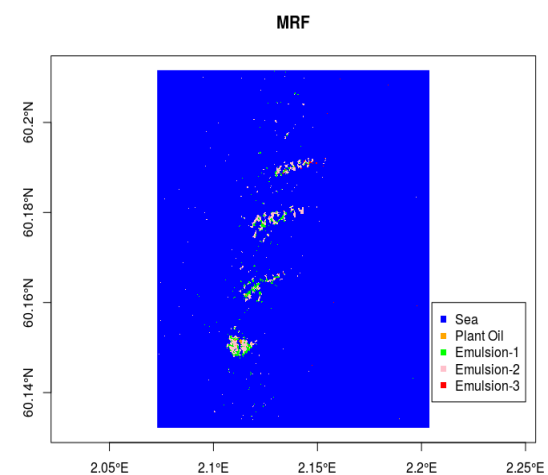


Figure 5: Classification results from MRF classification

Correspondingly, the results from MLC based MRF classification are reported in Figure 5. After tuning the parameters of the MRF classifier i.e. the values of lambda, initial temperature, and updating factor for reducing temperature came out to be 0.9, 3.2 and 0.85 respectively. There were 73 iterations for the MRF classifier. The trends for the temperature, kappa and energy can be observed in Figure 6. It is important to note that the value of kappa attained a maximum value at around iteration number 40 and then decreased gradually until the last iteration. After the full round of iterations, the value of kappa came out to be 0.266. The confusion matrix obtained after the classification is reported in Table 6. The matrix does not deviate too much from the one obtained from MLC results (Table 5). It also shows a reduced number of correctly classified pixels as compared to the MLC results.

On comparison of the results from MLC and MLC-MRF classification methods, we can state that MRF based classification method does not provide any improvement in the classification results. This could be attributed to the high incidence angle effect in the image which results in gradient of pixel values from high values on the right side of the image to lower values on the left side of the image for the same sea class.

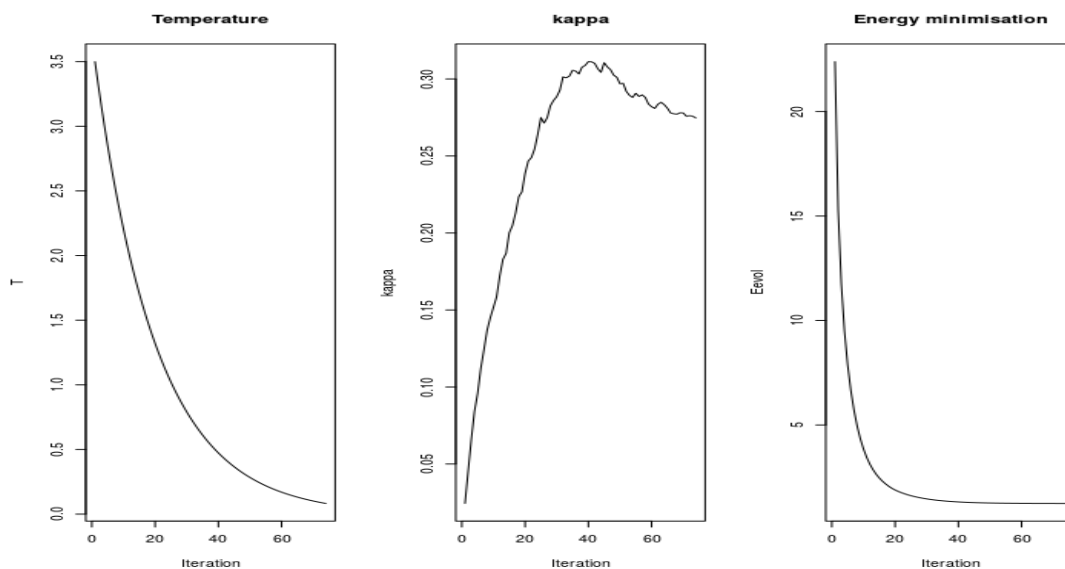


Figure 6: Variation of temperature, kappa, and energy with number of iterations

CONCLUSION

After assessment of the results from the two classifiers (Figure 4 and Figure 5) on this particular dataset (Figure 1), it can be concluded that both MLC and MLC-MRF classification methods are useful in separating oil spills from water. However, they are limited in their ability to distinguish between the type of oil spills (Table 5 and Table 6). It can also be concluded from Table 4 that SAR images are able to capture the dampening effect of oil on sea surface waves. The increasing amount of oil in the oil-slicks cause more dampening and hence better separability from seawater. The MRF classifier did not provide a significant improvement in the classification accuracy. The same method can give better classification results after including contextual features in the set of features provided to the classifier and correcting the incidence angle effect.

REFERENCES

- Alpers, W., Zhang, B., Mouche, A., Zeng, K., & Wai, P. (2016). Rain footprints on C-band synthetic aperture radar images of the ocean - Revisited. *Remote Sensing of Environment*, 187, 169–185. <https://doi.org/10.1016/j.rse.2016.10.015>
- Beyer, J., Trannum, H. C., Bakke, T., Hodson, P. V., & Collier, T. K. (2016). Environmental effects of the Deepwater Horizon oil spill: A review. *Marine Pollution Bulletin*, 110(1), 28–51. <https://doi.org/10.1016/j.marpolbul.2016.06.027>
- Brekke, C., Jones, C. E., Skrunes, S., Holt, B., Espeseth, M., & Eltoft, T. (2016). Cross-Correlation between Polarization Channels in SAR Imagery over Oceanographic Features. *IEEE Geoscience and Remote Sensing Letters*, 13(7), 997–1001. <https://doi.org/10.1109/LGRS.2016.2558543>
- Bulgarelli, B., & Djavidnia, S. (2012). On MODIS Retrieval of Oil Spill Spectral Properties in the Marine Environment. *IEEE Geoscience and Remote Sensing Letters*, 9(3), 398–402. <https://doi.org/10.1109/LGRS.2011.2169647>
- Chang, S. E., Stone, J., Demes, K., & Piscitelli, M. (2014). Consequences of oil spills: a review and framework for informing planning. *Ecology and Society*, 19(2). <https://doi.org/10.5751/ES-06406-190226>
- CNN. (2010). Oil Disaster by the numbers. Retrieved June 1, 2017, from <http://edition.cnn.com/SPECIALS/2010/gulf.coast.oil.spill/interactive/numbers.interactive/index.html>
- Dell'Amore, C. (2015, April 18). Why Did “Shocking” Amounts of BP Oil Fall to the Seafloor? Retrieved August 9, 2017, from <http://news.nationalgeographic.com/2015/04/150418-gulf-oil-spill-sea-snot-oceans-environment-energy-deepwater-bp/>

- Espeseth, M. M., Skrunes, S., Jones, C. E., Brekke, C., Holt, B., & Doulgeris, A. P. (2017). Analysis of Evolving Oil Spills in Full-Polarimetric and Hybrid-Polarity SAR. *IEEE Transactions On Geoscience and Remote Sensing*, 55(7), 4190–4210. <https://doi.org/10.1109/TGRS.2017.2690001>
- Fingas, M., & Brown, C. (2014). Review of oil spill remote sensing. *Marine Pollution Bulletin*, 83(1), 9–23. <https://doi.org/10.1016/j.marpolbul.2014.03.059>
- Gade, M., Alpers, W., Hühnerfuss, H., Masuko, H., & Kobayashi, T. (1998). Imaging of biogenic and anthropogenic ocean surface films by the multifrequency/multipolarization SIR-C/X-SAR. *Journal of Geophysical Research: Oceans*, 103(C9), 18851–18866. <https://doi.org/10.1029/97JC01915>
- Gens, R. (2008). Oceanographic Applications of SAR Remote Sensing. *GIScience & Remote Sensing*, 45(3), 275–305. <https://doi.org/10.2747/1548-1603.45.3.275>
- Kumar, S., Kattamuri, H. P., & Agarwal, S. (2016). Dark spot detection for characterization of marine surface slicks using PolSAR remote sensing. In *Proc. of SPIE* (Vol. 9878, p. 98780K1-17). <https://doi.org/10.1117/12.2224415>
- Liu, P., Zhao, C., Li, X., He, M., & Pichel, W. (2010). Identification of ocean oil spills in SAR imagery based on fuzzy logic algorithm. *International Journal of Remote Sensing*, 31(17–18), 4819–4833. <https://doi.org/10.1080/01431161.2010.485147>
- Lopez, L., & Moctezuma, M. (2005). Oil spill detection using GLCM and MRF. In *Geoscience and Remote Sensing Symposium, 2005. IGARSS '05. Proceedings. 2005 IEEE International* (pp. 1781–1784). <https://doi.org/10.1109/IGARSS.2005.1526349>
- Minchew, B., Jones, C. E., & Holt, B. (2012). Polarimetric Analysis of Backscatter From the Deepwater Horizon Oil Spill Using L-Band Synthetic Aperture Radar. *IEEE Transactions on Geoscience and Remote Sensing*, 50(10), 3812–3830. <https://doi.org/10.1109/TGRS.2012.2185804>
- Moctezuma, M., Parmiggiani, F., & Lopez, L. (2014). Measuring marine oil spill extent by Markov Random Fields. In *Proc. of SPIE* (Vol. 9240, p. 92400A1-6). <https://doi.org/10.1117/12.2068325>
- Morales, D. I., Moctezuma, M., & Parmiggiani, F. (2008). Detection of oil slicks in sar images using hierarchical MRF. *International Geoscience and Remote Sensing Symposium (IGARSS)*, 3(1), 1390–1393. <https://doi.org/10.1109/IGARSS.2008.4779620>
- NASA-JPL. (n.d.). Data Search - UAVSAR. Retrieved August 16, 2017, from <https://uavsar.jpl.nasa.gov/cgi-bin/data.pl>
- Pinel, N., & Bourlier, C. (2009). Unpolarized Infrared Emissivity Of Oil Films On Sea Surfaces. In *IEEE International Geoscience and Remote Sensing Symposium 2(2)* (pp. 1185–1188). <https://doi.org/10.1109/IGARSS.2009.5418007>
- Skrunes, S., Brekke, C., Jones, C. E., & Holt, B. (2016). A Multisensor Comparison of Experimental Oil Spills in Polarimetric SAR for High Wind Conditions. *IEEE Journal of Selected Topics in Applied Earth Observations and Remote Sensing*, 9(11), 4948–4961. <https://doi.org/10.1109/JSTARS.2016.2565063>
- Valenzuela, G. R. (1978). Theories for the interaction of electromagnetic and oceanic waves – a review. *Boundary Layer Meteorology*, 13, 61–85.
- Wang, D., Pan, D., Zhan, Y., & Zhu, Q. (2010). Experiment of monitoring oil spill on the base of EOS/MODIS data. In *SPIE – Int. Soc. Opt. Eng.* (Vol. 7831, p. 78311T). <https://doi.org/10.1117/12.864967>
- Weber, H. R. (2010). Blown-out BP well finally killed at bottom of Gulf. Retrieved June 1, 2017, from http://archive.boston.com/news/nation/articles/2010/09/19/blown_out_bp_well_finally_killed_at_bottom_of_gulf/